# Tailoring Microstructure and Superconducting Properties in Thick BaHfO$_3$ and Ba$_2$Y(Nb/Ta)O$_6$ Doped YBCO Films on Technical Templates

Max Sieger, Patrick Pahlke, Mayraluna Lao, Michael Eisterer, Alexander Meledin, Gustaaf Van Tendeloo, Rick Ottolinger, Jens Hänisch, Bernhard Holzapfel, Alexander Usoskin, Ahmed Kursumovic, Judith L. MacManus-Driscoll, Benjamin H. Stafford, Markus Bauer, Kornelius Nielsch, Ludwig Schultz, and Ruben Hühne

*(Invited Paper)*

*Abstract*—The current transport capability of YBa$_2$Cu$_3$O$_{7-x}$ (YBCO) based coated conductors (CCs) is mainly limited by two features: the grain boundaries of the used textured template, which are transferred into the superconducting film through the buffer layers, and the ability to pin magnetic flux lines by incorporation of defined defects in the crystal lattice. By adjusting the deposition conditions, it is possible to tailor the pinning landscape in doped YBCO in order to meet specific working conditions (*T*, *B*) for CC applications. To study these effects, we deposited YBCO layers with a thickness of about 1–2 $\mu$m using pulsed laser deposition on buffered rolling-assisted biaxially textured Ni-W substrates as well as on metal tapes having either an ion-beam-textured YSZ buffer or an MgO layer textured by inclined substrate deposition. BaHfO$_3$ and the mixed double-perovskite Ba$_2$Y(Nb/Ta)O$_6$ were incorporated as artificial pinning centers in these YBCO layers. X-ray diffraction confirmed the epitaxial growth of the superconductor on these templates as well as the biaxially oriented incorporation of the secondary phase additions in the YBCO matrix. A critical current density $J_c$ of more than 2 MA/cm² was achieved at 77 K in self-field for 1–2 $\mu$m thick films. Detailed TEM (transmission electron microscopy) studies revealed that the structure of the secondary phase can be tuned, forming *c*-axis aligned nanocolumns, *ab*-oriented platelets, or a combination of both. Transport measurements show that the $J_c$ anisotropy in magnetic fields is reduced by doping and the peak in the $J_c(\theta)$ curves can be correlated to the microstructural features.

*Index Terms*—Alternating beam assisted deposition (ABAD), coated conductors, inclined substrate deposition (ISD), pinning, pulsed laser deposition, RABiTS, YBa$_2$Cu$_3$O$_{7-x}$ (YBCO).

## I. Introduction

YBa$_2$Cu$_3$O$_{7-x}$ (YBCO) and related compounds are the basic materials for the realization of coated conductor (CC) applications. High-temperature superconductor (HTS) layers can be grown epitaxially onto different substrates by a number of physical and chemical deposition techniques, e.g. metal-organic chemical vapor deposition [1], electron-beam evaporation [2], pulsed laser deposition (PLD) [3]–[6] or chemical solution deposition [7]–[10]. Since grain boundaries (GBs) and texture are transferred by epitaxial growth into the HTS matrix, highly-oriented substrates/buffer layers are essential for high-$J_c$ performance of the functional layer in the low-field region, where GBs act as current blockers [11]–[15].

Over the last 20 years, significant efforts have been made to develop biaxially textured templates for long length conductor manufacture [16]. One of the technological approaches is the preparation of biaxially textured buffer layers on arbitrarily textured metal tapes by methods like ion-beam assisted deposition (IBAD) [17], [18], alternating beam assisted deposition (ABAD) [19] or inclined substrate deposition (ISD) [20]. Alternatively, highly textured metal templates are realized by the rolling-assisted biaxially textured substrate (RABiTS) approach [21]–[24].

More recently, significant efforts have been devoted to enhance the current transport capability of the superconducting

layers in magnetic fields. A variety of secondary particles were introduced into the YBCO matrix as perovskite-type Ba$MO_3$ ($M$ = Zr, Hf, Sn, ...) compounds [2], [6]–[8], [25]–[30] or double-perovskite oxides as $Ba_2YNbO_6$ [31], [32] or mixed $Ba_2Y(Nb_{0.5}Ta_{0.5})O_6$ (BYNTO) [33]–[36] to enhance vortex pinning and increase $J_c$ in high magnetic fields. A so-called nano-engineering, i.e. tailoring the amount, shape, size and arrangement of artificial pinning centers (APCs), gives the possibility to tune the $J_c(B, \theta)$ characteristic of a YBCO film to meet specific working conditions, e.g. wires at 77 K and $\leq 1$ T, wind turbines (30 K, $\sim$3-5 T) and high–field magnets (4.2 K, $>$5 T), making pinning-enhanced YBCO CCs superior to conventional superconducting wires.

In this work we investigate thick $BaHfO_3$ (BHO) and BYNTO-doped YBCO films deposited by PLD on buffered ABAD-YSZ templates, Ni-5at% W RABiTS substrates, as well as on ISD-MgO buffered Hastelloy tapes. We discuss the influence of growth rate, substrate temperature and doping level on the microstructure and electrical properties of the superconducting layer by means of electron microscopy, X-Ray diffraction, transport current measurements and scanning Hall probe microscopy (SHPM).

## II. EXPERIMENTAL DETAILS

### A. Sample Preparation

YBCO films with a thickness of more than 1 $\mu$m containing either up to 15 mol% of $BaHfO_3$ (BHO:YBCO) or 5 mol% of the mixed double-perovskite $Ba_2Y(Nb_{0.5}Ta_{0.5})O_6$ (BYNTO:YBCO) were deposited on technical substrates by pulsed laser deposition from premixed targets. A Lambda Physics LPX305Pro KrF excimer laser ($\lambda$ = 248 nm) was applied with varying repetition rates leading to a growth rate $R$ of 0.4 to 8 nm/s. More details can be found in Ref. [25], [26]. Three major types of coated conductor templates were studied, i.e. ABAD-YSZ-buffered stainless steel tape with a $CeO_2$ cap layer [37], CSD-$La_2Zr_2O_7$/$CeO_2$-buffered biaxially-textured Ni-5 at% W tape (RABiTS Ni-W, [35]), and ISD-MgO buffered Hastelloy tape with a 300 nm thin $GdBa_2Cu_3O_7$ seed layer [38]. The substrate temperature $T_s$ was varied between 770 and 840 °C via a resistive heater. A silver cap layer was deposited by PLD for surface protection and lower contact resistance during transport measurements.

### B. Structural Characterization

X-ray diffraction was carried out on a Bruker D8 Advance Diffractometer (Co-K$_\alpha$ radiation). High-angle annular dark field scanning transmission electron microscopy (HAADF-STEM), annular dark field scanning transmission electron microscopy (ADF-STEM) and energy-dispersive X-Ray spectroscopy (EDX) mappings were performed on an *FEI Tecnai Osiris* microscope operated at 200 kV as well as on an *FEI Titan* "cubed" electron microscope operated at 200 kV and 300 kV.

### C. Electrical Characterization

The critical temperature $T_{c,90}$ was measured inductively (transition width $\Delta T_c = T_{c,90} - T_{c,10}$). Maps for the critical

TABLE I
STRUCTURAL AND ELECTRICAL PROPERTIES OF PRISTINE YBCO, BHO:YBCO AND BYNTO:YBCO FILMS ON ABAD-YSZ ($T_s$ = 810 °C, $R$ = 1.3 nm/s)

| Parameter | YBCO | BHO:YBCO | BYNTO:YBCO |
|---|---|---|---|
| YBCO $c$-axis, Å | 11.72 | 11.76 | 11.74 |
| $T_{c,90}$ ($\Delta T_c$), K | 89.0 (1.0) | 87.5 (2.0) | 91.0 (2.0) |
| $J_{c,sf}$ (77 K), MA/cm$^2$ | 2.3 $\pm$ 0.2 | 0.8 $\pm$ 0.2 | 2.1 $\pm$ 0.2 |
| $Y_2O_3$ precipitates | present [37] | reduced | increased |

current density ($J_c$) distribution in the sample were obtained by inversion of the trapped field profile measured by a scanning Hall probe device (scanning Hall probe microscopy, SHPM, [39]) in liquid $N_2$ (77 K). The listed values correspond to the self-field (sf) critical current density $J_{c,sf}$. Angle-resolved critical current density measurements in magnetic fields, $J_c(B, \theta)$, were carried out by either using a vector vibrating sample magnetometer (VSM) or by transport measurements. The latter were conducted in maximum Lorentz force configuration in a four-point measurement assembly using laser-cut bridges of 800 $\mu$m length and 300 to 500 $\mu$m width. Here, $J_c$ is defined by an electrical field criterion of 1 $\mu$V/cm. In both cases, $\theta$ is the angle between the magnetic field $\vec{B}$ and the sample normal $\vec{n}$ ($\vec{B}\|\vec{n}$ for 0° and 180°, $\vec{B}\perp\vec{n}$ for 90°).

## III. RESULTS AND DISCUSSION

### A. Films on ABAD-YSZ

YBCO samples with 6 mol% BHO (2.6 vol%) and 5 mol% BYNTO (4.7 vol%) respectively were deposited on ABAD-YSZ substrates using $T_s$ = 790 to 830 °C and $R$ = 0.4 to 1.3 nm/ s. At first, we start to discuss samples prepared with standard deposition conditions ($T_s$ = 810 °C, $R$ = 1.3 nm/ s) having a film thickness $\sim$1.2 $\mu$m. Typical results of the structural and electrical characterization are summarized in Table I for those samples. The $\theta$-$2\theta$ scans reveal a pure $c$-axis growth of YBCO, BHO and BYNTO. It was proven by texture measurements and TEM analysis that BHO and BYNTO are incorporated biaxially textured into the YBCO matrix resulting in an elongation of $c_{YBCO}$ (see Table I). Compared to $T_c$ = 89.0 K for the undoped sample, $T_c$ is lower in the BHO-doped film (87.5 K), but higher for the BYNTO sample (91.0 K). $J_{c,sf}$ (77 K) is reduced to about 40% of the value of pure YBCO by doping with BHO, but almost not changed by doping with BYNTO. We find a comparatively high density of nanosized $Y_2O_3$ platelets in pristine YBCO, which is usual for our films [37]. The amount of $Y_2O_3$ is strongly reduced by BHO additions. In contrast, a increased concentration was detected in the BYNTO samples (see Fig. 1).

We found that the local microstructure and therefore the $J_c$ anisotropy are sensitive to deposition conditions such as growth rate ($R$) and substrate temperature ($T_s$). The microstructure for different $R$ is shown in Fig. 2 as one example. Aside from the BHO nanostructures, we will focus on defect structures like $YBa_2Cu_4O_8$ (Y-124) intergrowths and nanometer-sized $Y_2O_3$ precipitates. At low $R$, BHO grows as almost pure fan-shaped nanocolumns. By increasing $R$, BHO columns become straighter so that fan-shaped and straight parts coexist. It was shown before
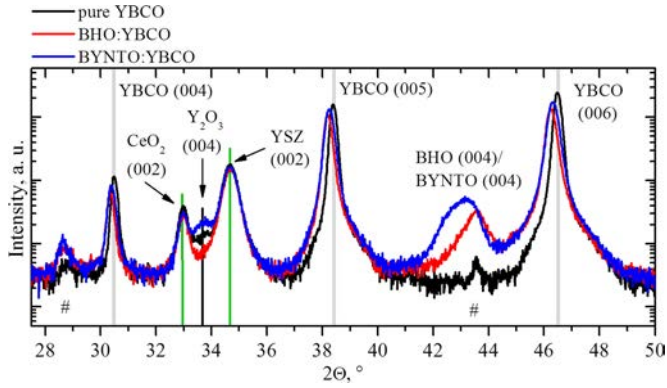
Fig. 1. Θ-2Θ scans for YBCO, BHO:YBCO and BYNTO:YBCO deposited on ABAD-YSZ at $T_s = 810\,°C$ and $R = 1.3\,nm/s$ (# denote peaks from the underlying metal tape).
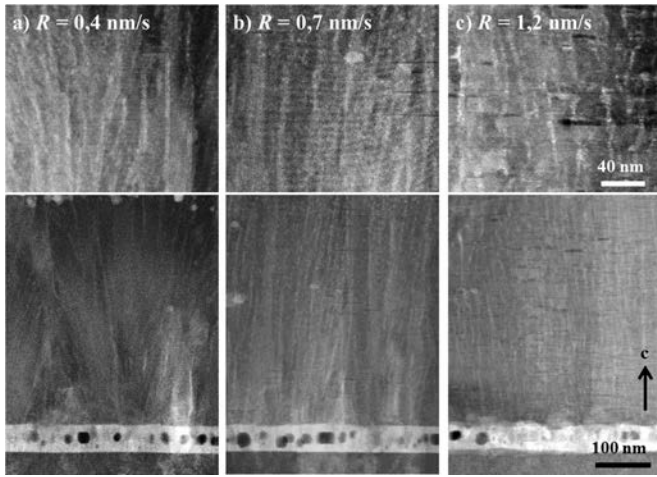


Fig. 2. ADF-STEM images of BHO:YBCO samples on ABAD-YSZ prepared at $T_s \sim 800\,°C$ and growth rates of $R = 0.4, 0.7$ and $1.2\,nm/s$. Top: BHO:YBCO bulk region (higher magnification). Bottom: BHO:YBCO/tape interface region. The dark spots in the bright $CeO_2$-layer are Ba-rich precipitates.
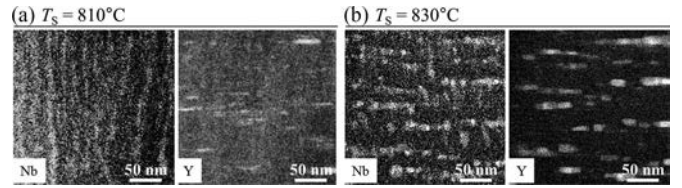


Fig. 3. STEM-EDX elemental mappings of Nb and Y for BYNTO:YBCO samples deposited at (a) 810 °C and (b) 830 °C on ABAD-YSZ using a deposition rate of $R = 1.3\,nm/s$.
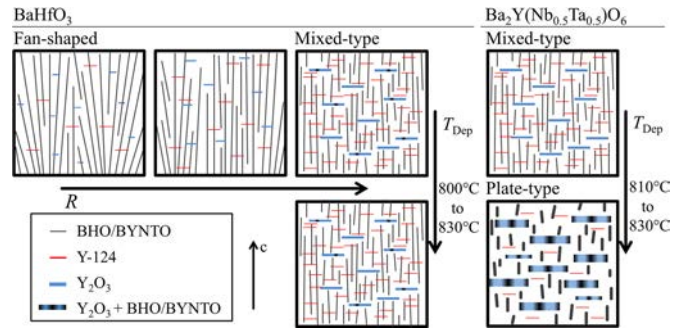


Fig. 4. Scheme of different types of defect structure for BHO and BYNTO doped YBCO films deposited on ABAD-YSZ templates at growth rate $R = 0.4$-$1.3\,nm/s$ and temperatures $T_s = 800$-$830\,°C$.
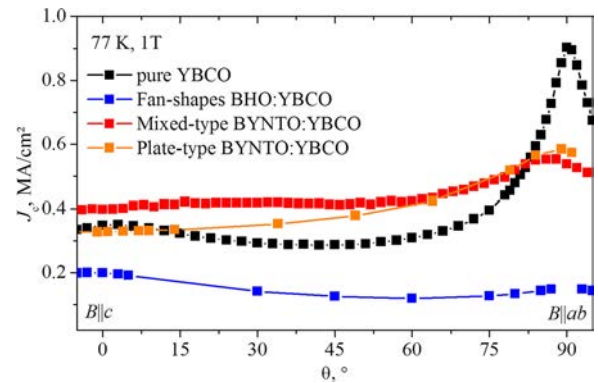


Fig. 5. Angular dependence of the critical current density, $J_c(\theta)$, at 77 K / 1 T of fan-shaped BHO:YBCO and mixed-type and plate-type BYNTO:YBCO samples deposited on ABAD-YSZ.

that the splay of $BaZrO_3$ nanocolums is also influenced by the substrates temperature [40] and surface [41].

The density of Y-124 intergrowth is low and $Y_2O_3$ platelets with a size <10 nm are dispersed in the YBCO matrix. At $R>1\,nm/s$, the $c$-axis aligned BHO columns get shorter and the amount of $ab$-aligned $Y_2O_3$ platelets is increased. The local microstructure is generally more disordered and the density of Y-124 intergrowths is higher compared to deposition at lower growth rates. The mixture of $ab$-aligned and $c$-axis aligned nanostructures was already shown by Ercolano et al. [33] and will be called "mixed-type" structure in the following discussion.

A microstructure, which is similar to that of BHO:YBCO at $R > 1\,nm/s$, was also found in BYNTO:YBCO samples using a similar temperature, $T_s = 810\,°C$, and growth rate, $R = 1.3\,nm/s$ (compare Fig. 2(c) and 3(a)).

Here, a mixed-type structure is formed consisting of >100 nm long BYNTO columns and about 10 nm × 20 nm large $Y_2O_3$

platelets (Fig. 3 a)). When increasing $T_s$ by about 20 K, the density and length of the $c$-axis oriented BYNTO columns as well as the density of Y-124 intergrowth is significantly reduced whereas 20 nm × 50 nm sized BYNTO/$Y_2O_3$ mixed $ab$-aligned platelets are formed (plate-type, Fig. 3 (b)). In contrast, the microstructure did not change significantly for higher $T_s$ in the BHO doped samples. As a summary of these observations, Fig. 4 presents a schematic overview, how number, size and orientation of dopant, Y-124 and $Y_2O_3$ change with increasing $R$ and $T_s$.

Fig. 5 gives the anisotropy curves at 77 K, 1 T for a fan-shape type BHO sample as well as the mixed-type and plate-type BYNTO samples in comparison with undoped YBCO. The absolute values of $J_c(\theta)_{min}$ for the BYNTO-doped films
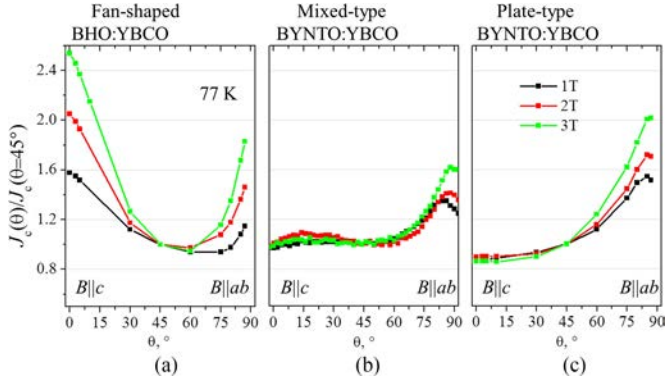
Fig. 6. Angular dependence of the critical current density, $J_c(\theta)$, of (a) fan-shaped BHO:YBCO, mixed-type BYNTO:YBCO and plate-type BYNTO:YBCO samples deposited on ABAD-YSZ. Data for (a) and (c) were obtained by VSM measurements, for (b) by transport measurement. $J_c$ data were taken at 77 K and normalized to $J_c(\theta = 45°)$.

are higher than in the undoped sample. At these conditions the $J_c$-performance of the fan-shaped BHO-doped sample is lower compared to the undoped sample. The situation is different at lower temperatures and higher field (40 K / 4 T), where this type of pinning centers was found to be more effective [26].

Fig. 6 summarizes the corresponding normalized $J_c$ anisotropy curves at 77 K: The fan-shaped BHO nanocolumns create a broad peak in $J_c(\theta)$ at $B\|c$ (Fig. 6(a)). A detailed discussion of the $J_c(B, \theta, T)$-behavior is given in Ref. [26].

In the mixed-type BYNTO sample, where $c$-axis correlated defects and $ab$-aligned BYNTO/$Y_2O_3$ platelets are present, only small peaks at $B\|c$ and $B\|ab$ are found in the anisotropy curve (Fig. 6(b)). In general, $J_c$ is enhanced over a wide angular range whereas the anisotropy $J_c(\theta)_{max}/J_c(\theta)_{min}$ is well below two for fields up to 3 T in the measured temperature range of 40 to 77 K. This might be a result of the simultaneously acting $c$-axis and $ab$-axis aligned defects, leading to enhanced pinning at angles $\theta$ between 0° and 90° (staircase model in Ref. [33]). $J_{c,min}$ is enhanced by more than 50% compared to similar undoped samples especially at $T < 77$ K (data not shown).

In contrast, the BYNTO:YBCO sample prepared at higher $T_s$ exhibits a strong and broad peak for $B\|ab$ and virtually no peak for $B\|c$ (Fig. 6(c)). This might be explained by the fact that almost no $c$-axis correlated defects are present, whereas a high number of $ab$-aligned BYNTO/$Y_2O_3$ platelets are found.

### B. Films on RABiTS Ni-W

Doped YBCO films on buffered Ni-W tapes show a similar microstructure to that of films on ABAD-YSZ tapes with the exception of the additional global grain network arising from the template ($\sim$20 to 50 $\mu$m diameter grains on Ni-W, $<1$ $\mu$m on ABAD-YSZ [42]). Strong (00$\ell$) peaks in XRD measurements (data not shown) indicate a highly $c$-axis oriented growth; additional peaks of the dopant material appear for the 5 mol% BHO (2.2 vol%) and BYNTO doped samples. The 15 mol% BHO (6.9 vol%) doped sample shows an asymmetric BHO peak shape which might be associated with the incorporation of Y in BHO or Hf in $Y_2O_3$, respectively [25], [43], [44]. The biaxially

TABLE II
STRUCTURAL AND ELECTRICAL PROPERTIES OF PRISTINE YBCO, BHO:YBCO AND BYNTO:YBCO FILMS PREPARED WITH STANDARD CONDITIONS ON NI-5W

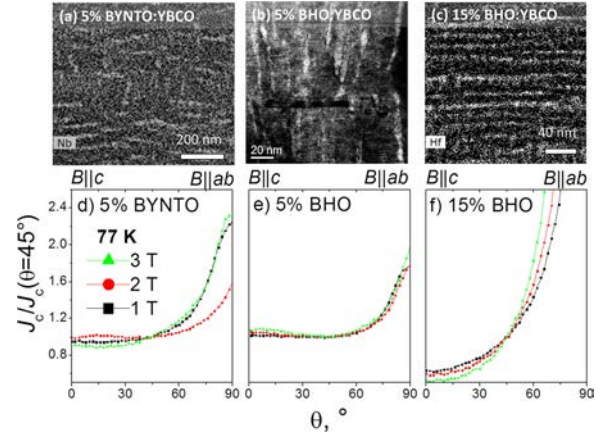| Parameter | YBCO | +5BYNTO | +5BHO | +15BHO |
|---|---|---|---|---|
| YBCO $c$-axis, Å | 11.69 | 11.71 | 11.72 | 11.74 |
| $T_{c,90}$ ($\Delta T_c$), K | 90.4 (1.2) | 90.1 (1.0) | 88.3 (0.8) | 88.0 (2.1) |
| $Y_2O_3$ precipitates | present | increased | reduced | reduced |



Fig. 7. Spatial distribution of BYNTO and BHO in (a) 5 mol% BYNTO, (b) 5 mol% BHO and (c) 15 mol% BHO doped YBCO films, observed as bright contrast in (b) HAADF-STEM and (d)-(f) STEM-EDX elemental mappings with respective normalized $J_c$ anisotropy curves at 77 K for several magnetic fields (All films deposited at 830 °C on Ni5W, $R = 1.6$ nm/s).

oriented BHO nanoparticles lead to an elongation of the YBCO $c$-axis, a reduction of $T_c$ and a suppression of the $Y_2O_3$ formation. In comparison, BYNTO-doped films exhibit only a slight increase in $c$-axis length, slightly decreased $T_c$ and a preferred formation of $Y_2O_3$ (Table II) as on ABAD-YSZ (Table I)

In BYNTO doped YBCO films on Ni-W the used growth conditions lead to a mixed-type structure of $c$-axis aligned BYNTO columns and $ab$-aligned $Y_2O_3$ platelets (partly with Nb and Ta additions, Fig. 7(a)) similar to films on ABAD-YSZ (cf. Fig. 3(b)). The local microstructure of the 5 mol% BHO doped samples is similar to that observed for ABAD-YSZ based films (Fig. 2(c)). At $T_s = 830$ °C and growth rates of $R \sim 1.6$ nm/s, $c$-axis aligned columns are formed (Fig. 7(b)). A higher content of 15 mol% BHO leads to the formation of incomplete BHO and/or $Y_2O_3$ layers within the YBCO matrix mainly parallel to the $ab$-plane (Fig. 7(c)). A minor BHO component of $c$-axis oriented columns with a fan-shaped structure is also present in these samples. In addition to the deposition parameters, the microstructure might depend on the vicinal angle of the underlying substrate [42], [43]. As the grains on RABiTS Ni-W exhibit an individual tilt of the Ni-W [001] direction towards the tape normal, an additional grain to grain variance of the microstructure cannot be excluded.

This particular microstructures lead to a specific in-field current transport behavior. Fig. 7 (d)–(f) show normalized anisotropy curves at 77 K for magnetic fields up to 3 T, where $J_c/J_c(\theta = 45°)$ is a measure for the strength of correlated
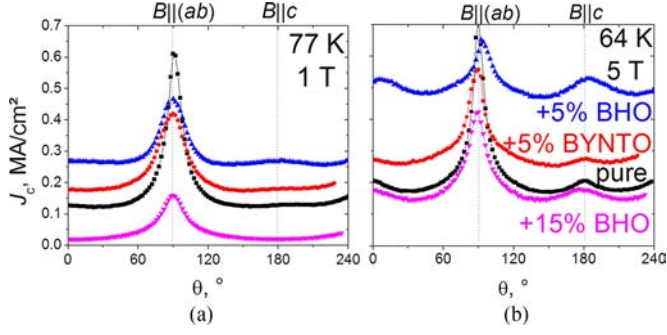
Fig. 8. Angular dependence of $J_c$ at (a) 77 K / 1 T and (b) 64 K / 5 T for pure YBCO, BYNTO, low BHO and highly BHO doped YBCO films deposited at 830 °C on Ni5W, $R = 1.6$ nm/s.

TABLE III
ANISOTROPY $J_{c,max} / J_{c,min}$ OF PRISTINE YBCO, BHO:YBCO AND BYNTO:YBCO FILMS PREPARED WITH STANDARD CONDITIONS ON RABiTS NI-W

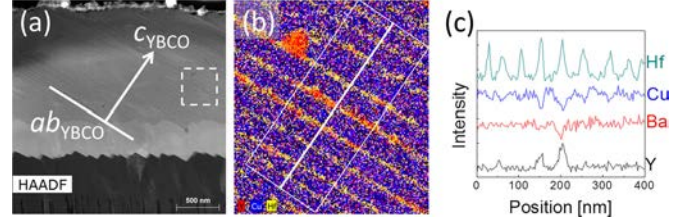| Measurement conditions | YBCO | +5BYNTO | +5BHO | +15BHO |
|---|---|---|---|---|
| 77 K / 1 T | 5.1 | 2.5 | 1.8 | 8.4 |
| 64 K / 5 T | 4.2 | 2.2 | 1.4 | 1.2 |



Fig. 9. (a) HAADF-STEM image together with (b) STEM-EDX mapping and (c) integrated element line scan of Hf, Cu, Ba, Y (green, blue, red and black respectively) of 10 mol% BHO:YBCO on ISD-MgO. (HAADF STEM image showing the mapped area by a white square, the composite STEM-EDX mapping showing the area of the integrated line scan by a white rectangle.)
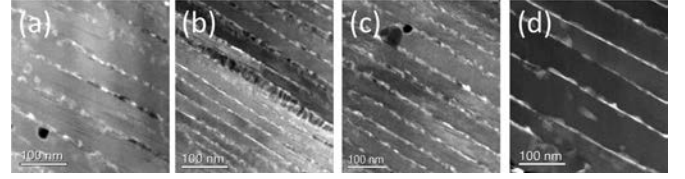


Fig. 10. ADF-STEM images of a 5 mol% BHO:YBCO films deposited at (a) 810 °C, (b) 10 mol% BHO / 770 °C, (c) 10 mol% BHO / 810 °C, (d) 10 mol% BHO / 840 °C on ISD-MgO.

pinning centers parallel to the $c$-axis ($\theta = 0°$) and $ab$-planes ($\theta = 90°$). All samples show only weak $c$-axis correlated pinning at 77 K in the examined magnetic field range up to 3 T, i.e. $J_c^{B\|c}/J_c(45°) \sim 1$, as is apparent in the $J_c(\theta)$ curve at 77 K at 1 T (Fig. 8(a)). Whereas BYNTO doped and low BHO concentration YBCO films show moderate pinning for $B\|ab$ ($\sim$2.5), the highly BHO-doped film with $ab$-parallel platelets exhibits a strong anisotropy, i.e. $J_c^{B\|ab}/J_c(45°)$ ranges up to 15 at 3 T.

The $J_c$ measurements at 77 K, 1 T (Fig. 8(a)) and 64 K, 5 T (Fig. 8(b)) show a decreased anisotropy $A = J_{c,max}/J_{c,min}$ (cf. Table III) for all doped films on RABiTS Ni-W compared to the pure YBCO as desired for specific applications such as superconducting magnets. At 77 K / 1 T both low-doped films perform better than pure YBCO in a wide angular range. The 15 mol% BHO doped YBCO shows reduced $J_c$ values in the full angular range with a high anisotropy ($A = 8.4$). The reduced $J_c$ values might be due to the broad $\Delta T_c$ and small irreversibility fields $H_{irr}$ in $c$-direction.

At lower temperatures, the nanosized structures lead to characteristic pinning effects for magnetic fields with an additional broad peak for $B\|c$. The highly-BHO doped sample almost reaches the $J_c$ level of pure YBCO. The critical current density of the 5% BYNTO-doped YBCO is significantly increased in a wide angular range compared to pure YBCO by the wide-angle pinning ability of the mixed-type structures. The peak for $B\|c$ of the 5% BHO:YBCO film is massively increased by the $c$-axis oriented BHO nanocolumns. This sample shows the best performance with a high $J_c$ level in the full angular range.

## C. Films on ISD-MgO

Although we were able to grow high-quality YBCO films with $c$-axis oriented nanostructures on textured metal tapes and textured ABAD-based buffer layers by proper adjustment of the growth parameters $T$ and $R$, these results are not directly transferable to PLD-BHO:YBCO films on ISD-MgO buffered templates, which have an inherent tilt of the [001] direction away from the tape normal of $\sim$30°. The epitaxial, yet tilted growth (proven by pole figure measurements, not shown here) of the BHO:YBCO film on such substrates leads to the formation of a layered structure parallel to the $ab$-plane adopting the tilt angle of the template (Fig. 9 (a)). The elemental mapping for Y, Cu and Hf (Fig. 9 (b)+(c)) indicates a stacking of YBCO layers and BHO/$Y_2O_3$ platelets. An incorporation of Hf in $Y_2O_3$ or Y in BHO cannot be excluded from these data.

In order to understand the growth mode on ISD templates, BHO:YBCO films have been grown on vicinal-cut $SrTiO_3$ single crystals with vicinal angles $\alpha$ from 0 to 40° [43]. Whereas BHO:YBCO films on flat (0°) STO substrates exhibit columnar BHO structures parallel to $c_{YBCO}$, low miscut angles (2 to 10°) lead to mixed-type structures similar to Fig. 3 and Fig. 7(a). This is also in accordance with results of Baca et al. studying thin $BaZrO_3$-doped YBCO films on vicinal tilted single crystals [41], [45]. Even higher angles $\alpha$ lead to tilted BHO/$Y_2O_3$ platelets as observed for BHO:YBCO/ISD-MgO. Such structures were found to significantly decrease $J_c$ values in longitudinal direction and increase the anisotropy by current blocking [46].

For BHO:YBCO films on ISD-MgO different deposition parameters were varied to test if a different distribution of the incorporated pinning centers can be realized. It was found that the thickness and distance of the BHO/$Y_2O_3$ layers can be adjusted by the doping content and the temperature $T_S$. A higher growth temperature leads to enhanced diffusion and thereby wider separation (distance $d$) between the platelet regions (Fig. 10), whereas the thickness $t$ of these platelets is barely influenced (Table IV).

TABLE IV
THICKNESS AND DISTANCE OF BHO/$Y_2O_3$ PLATELETS IN BHO:YBCO FILMS ON ISD-MgO TAPES

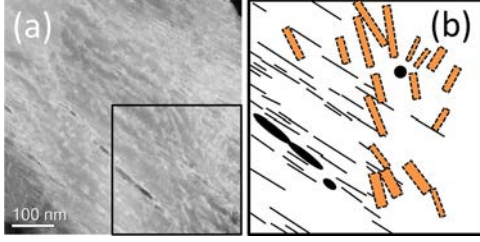| BHO CONTENT, mol% | DEPOSITION TEMPERATURE, °C | DISTANCE, nm | THICKNESS, nm | $T_{c,90}$ ($\Delta T_c$), K |
|---|---|---|---|---|
| 5 | 810 | 80-90 | 15 | 88.8 (1.1) |
| 10 | 770 | 30 | 5-6 | 87.9 (0.8) |
| 10 | 810 | 50 | 5-10 | 88.7 (1.6) |
| 10 | 840 | 75 | 7-10 | 88.3 (2.1) |



Fig. 11. (a) ADF-STEM image of a 5% BHO:YBCO film on ISD-MgO (deposition conditions $T_s = 770\,°C$, $R = 5.4\,nm/s$). (b) The microstructural features of the inset are sketched including large $Y_2O_3$ precipitates (black ellipsoids), extra $CuO_2$ chains (black lines) and short BHO columns (orange rectangles).
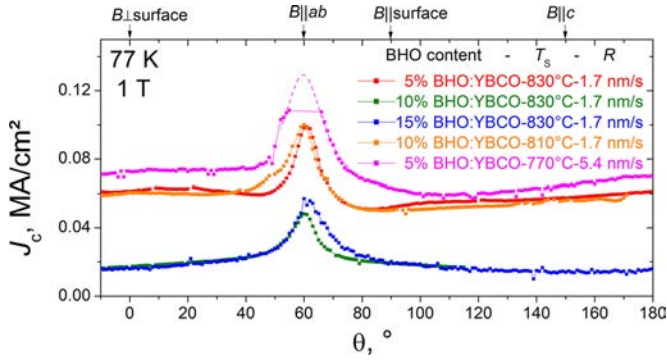


Fig. 12. Critical current anisotropy, $J_c(\theta)$, at 77 K, 1 T for PLD-BHO:YBCO films with different BHO contents on ISD-MgO templates deposited at different $T_S$ and $R$ (color code according to Ref. [2], purple curve fitted by a Lorentz function for $\theta = 55\,to\,65°$ as $I_c$ exceeded the measurement current of the set-up).

Doubling the BHO content in the YBCO matrix at the same $T_S$ leads to almost half the distance $t$ between adjacent BHO platelets. Higher growth rates $R$ tilt the BHO platelets towards the $c_{YBCO}$ (Fig. 11, BHO sketched as orange rectangles in Fig. 11(b)). Additionally a lot of extra $CuO_2$ planes (i.e. Y-124) as well as some larger $Y_2O_3$ agglomerates appear. At very high $R$ (8 nm/s) a highly lamellar growth in the direction of the substrate normal leads to porous films by shadowing effects (not shown here). All three parameters do not influence the $c$-axis length ($\sim$11.8 Å) and do only marginally decrease $T_c$ from the value of a pure YBCO film on ISD-MgO ($T_S = 810\,°C$, $R = 1.6\,nm/s$) with $T_{c,90} = 89.5$ K, $\Delta T_c = 0.9$ K (cf. Table IV).

The critical current anisotropy curves (Fig. 12) are highly influenced by the deposition conditions $T_S$, $R$ and the BHO content of the BHO:YBCO films. All films show a strong $ab$-plane correlated pinning behavior. Medium (10%, green) and high (15%, blue) BHO levels show lower absolute $J_c$ values than

the low doped (5%, red) BHO:YBCO film. This is comparable to films deposited by electron-beam evaporation (cf. *Stafford et al.* [2], 4.5 mol%, 8.6 mol% and 12.9 mol% BHO:YBCO, same color code). The $J_c(\theta)$ curves of medium (green) and high BHO:YBCO (blue) are symmetrical to the $ab$-peak. The high-$R$ sample (purple) exhibits a plateau between $B\perp$surface and $B\|ab$, probably caused by pinning-active particle species tilted off the $ab$-plane (cf. Fig. 11). The same argument holds for the low BHO:YBCO (red) sample that shows a broad peak around $\theta\sim15$ to $20°$, and the medium-BHO:YBCO sample deposited at reduced $T_S$ (orange), where decreased diffusion might form pinning species off the $ab$-plane.

## IV. CONCLUSION

As the presented results show, it is possible to tailor the microstructure in thick BHO and BYNTO doped YBCO films on technical templates by careful adjustment of key parameters such as substrate temperature $T_S$, growth rate $R$ and doping level. On ABAD-YSZ templates we were able to create pinning centers acting effectively for $B\|c$ or $B\|ab$. Moreover a mixed type could be realized with low $J_c$ anisotropy, which is explained by the observed microstructure. Similar microstructures were found on Ni5-W templates. Low doping contents of BHO and BYNTO (5 mol%) lead to either $c$-axis aligned or mixed-type structures with improved $J_c(\theta)$ performance. A higher concentration of BHO results in BHO/$Y_2O_3$ platelets oriented parallel to the $ab$-plane. This sample shows an increased anisotropy at high temperatures. The growth of APCs on ISD-MgO-based templates is mainly influenced by the lattice tilt of the substrate that is inherited by the YBCO layer, which leads to layered structures parallel to the $ab$-planes. It is possible to change the distance of such planes by growth temperature and doping level, the orientation is dependent on diffusion processes and therefore $R$ and $T_S$ Short and strongly splayed BHO nanocolumns are formed at high growth rate and low substrate temperature leading to superior $J_c(\theta)$ behavior.

## REFERENCES

[1] V. Selvamanickam *et al.*, "Enhanced critical currents in (Gd,Y)Ba$_2$Cu$_3$O$_x$ superconducting tapes with high levels of Zr addition," *Supercond. Sci. Technol.*, vol. 26, Jan. 2013, Art. no. 035006.

[2] B. Stafford *et al.*, "Pinning centres in ISD-MgO coated conductors via EB-PVD," *IEEE Trans. Appl. Supercond.*, vol. 26, no. 3, Apr. 2016, Art. no. 6601105.

[3] X. D. Wu *et al.*, "Epitaxial ordering of oxide superconductor thin films on (100) SrTiO$_3$ prepared by pulsed laser evaporation," *Appl. Phys. Lett.*, vol. 51, no. 11, 861–863, 1987.

[4] M. Peurla, H. Huhtinen, P. Paturi, Yu P. Stepanov, J. Raittila, and R. Laiho, "YBCO films prepared by PLD using nanocrystalline targets doped with BaZrO$_3$ or Y211," *IEEE Trans. Appl. Supercond.*, vol. 15, no. 2, pp. 3050–3053, Jun. 2005.

[5] A. Usoskin and H. C. Freyhardt, "YBCO-Coated conductors manufactured by high-rate pulsed laser deposition," *MRS Bulletin*, vol. 29, no. 8, pp. 583–589, 2004.

[6] M. Sieger *et al.*, "Pulsed laser deposition of thick $BaHfO_3$-doped $YBa_2Cu_3O_{7-\delta}$ films on highly alloyed textured Ni-W tapes," *J. Phys.: Conf. Ser.*, vol. 507, 2014, Art. no. 022032.

[7] S. Engel, T. Thersleff, R. Hühne, L. Schultz, and B. Holzapfel, "Enhanced flux pinning in $YBa_2Cu_3O_7$ layers by the formation of nanosized $BaHfO_3$ precipitates using the chemical deposition method," *Appl. Phys. Lett.*, vol. 90, Feb. 2007, Art. no. 102505.

[8] M. Erbe *et al.*, "Improved $REBa_2Cu_3O_{7-x}$ (RE = Y, Gd) structure and superconducting properties by addition of acetylacetone in TFA-MOD precursor solutions," *J. Mater. Chem. A*, vol. 2, pp. 4932–4944, Jan. 2014.

[9] M. Coll *et al.*, "Size-controlled spontaneously segregated $Ba_2YTaO_6$ nanoparticles in $YBa_2Cu_3O_7$ nanocomposites obtained by chemical solution deposition," *Supercond. Sci. Technol.*, vol. 27, Jan. 2014, Art. no. 044009.

[10] P. Cayado *et al.*, "Epitaxial $YBa_2Cu_3O_{7-x}$ nanocomposite thin films from colloidal solutions," *Supercond. Sci. Technol.*, vol. 28, Nov. 2015, Art. no. 124007.

[11] D. T. Verebelyi *et al.*, "Low angle grain boundary transport in $YBa_2Cu_3O_{7-\delta}$ coated conductors," *Appl. Phys. Lett.*, vol. 76, no. 13, 1755–1757, Mar. 2000.

[12] J. H. Durrell, M. J. Hogg, F. Kahlmann, Z. H. Barber, M.G. Blamire, and J. E. Evetts, "Critical current of $YBa_2Cu_3O_{7-\delta}$ low-angle grain boundaries," *Phys. Rev. Lett.*, vol. 90, no. 24, Jun. 2003, Art. no. 247006.

[13] J. H. Durrell and N. A. Rutter, "Importance of low-angle grain boundaries in $YBa_2Cu_3O_{7-\delta}$ coated conductors," *Supercond. Sci. Technol.*, vol. 22, 2009, Art. no. 013011.

[14] D. Dimos, P. Chaudhari, J. Mannhart, and F. K. LeGoues, "Orientation dependence of grain-boundary critical currents in $YBa_2Cu_3O_{7-\delta}$ bicrystals," *Phys. Rev. Lett.*, vol. 61, 219–222, Jul. 1988.

[15] L. Fernández *et al.*, "Influence of the grain boundary network on the critical current of $YBa_2Cu_3O_7$ films grown on biaxially textured metallic substrates," *Phys. Rev. B*, vol. 67, 2003, Art. no. 052503.

[16] X. Obradors and T. Puig, "Coated conductors for power applications: materials challenges," *Supercond. Sci. Technol.*, vol. 27, Mar. 2014, Art. no. 044003.

[17] Y. Iijima, N. Tanabe, Y. Ikeno, and O. Kohno, "Biaxially aligned $YBa_2Cu_3O_{7-x}$ thin film tapes," *Physica C*, 185–189, 1959–1960, 1991.

[18] K. Hasegawa *et al.*, "In-plane aligned YBCO thin film tape fabricated by pulsed laser deposition," in *Proc. 16th Int. Cryogenic Eng. Conf./Int. Cryogenic Mater. Conf.*, Amsterdam: Elsevier Science, 1997, pp. 1413–1416.

[19] A. Usoskin *et al.*, "Processing of long-length YBCO coated conductors based on stainless steel tapes," *IEEE Trans. Appl. Supercond.*, vol. 17, no. 2, pp. 3235–3238, Jun. 2007.

[20] M. Bauer, R. Semerad, and H. Kinder, "YBCO films on metal substrates with biaxially aligned MgO buffer layers," *IEEE Trans. Appl. Supercond.*, vol. 9, no. 2, pp. 1502–1505, Jun. 1999.

[21] J. Eickemeyer, D. Selbmann, R. Optiz, E. Maher, and W. Prusseit, "Effect of nickel purity on cube texture formation in RABiT-tapes," *Phys. C Supercond.*, vol. 341–348, pp. 2425–2426, Nov. 2000.

[22] U. Gaitzsch *et al.*, "Highly alloyed Ni-W substrates for low AC loss applications," *Supercond. Sci. Technol.*, vol. 26, no. 8, Jul. 2013, Art. no. 085024.

[23] J. Eickemeyer *et al.*, "Textured Ni-9.0% W substrate tapes for YBCO-coated conductors," *Supercond. Sci. Technol.*, vol. 23, no. 8, Jul. 2010, Art. no. 085012.

[24] R. Hühne, V. Subramanya Sarma, D. Okai, T. Thersleff, L. Schultz, and B. Holzapfel, "Preparation of coated conductor architectures on Ni composite tapes," *Supercond. Sci. Technol.*, vol. 20, no. 7, pp. 709–714, Jun. 2007.

[25] M. Sieger *et al.*, "$BaHfO_3$-doped thick $YBa_2Cu_3O_{7-\delta}$ films on highly alloyed textured Ni-W tapes," *IEEE Trans. Appl. Supercond.*, vol. 25, no. 3, Jun. 2015, Art. no. 6602604.

[26] P. Pahlke *et al.*, "Reduced $J_c$ anisotropy and enhanced in-field performance in thick $BaHfO_3$-doped $YBa_2Cu_3O_{7-\delta}$ films on ABAD-YSZ templates," *IEEE Trans. Appl. Supercond.*, vol. 26, no. 3, Apr. 2016, Art. no. 6603104.

[27] A. Kiessling *et al.*, "Nanocolumns in $YBa_2Cu_3O_{7-x}$/$BaZrO_3$ quasi-multilayers: formation and influence on superconducting properties," *Supercond. Sci. Technol.*, vol. 24, no. 5, Mar. 2011, Art. no. 055018.

[28] J. Hänisch *et al.*, "Formation and pinning properties of growth-controlled nanoscale precipitates in $YBa_2Cu_3O_{7-\delta}$/transition metal quasi-multilayers," *Supercond. Sci. Technol.*, vol. 19, no. 6, pp. 534–540, Apr. 2006.

[29] Tsuruta *et al.*, "Effect of $BaHfO_3$ introduction on the transport current at the grain boundaries in $SmBa_2Cu_3O_y$ films," *Appl. Phys. Exp.*, vol. 8, 2015, Art. no. 033101.

[30] J. L. MacManus-Driscoll *et al.*, "Strongly enhanced current densities in superconducting coated conductors of $YBa_2Cu_3O_{7-x}$ + $BaZrO_3$," *Nature Mater.*, vol. 3, pp. 439–443, Jul. 2004.

[31] D. M. Feldmann, T. G. Holesinger, B. Maiorov, S. R. Foltyn, J. Y. Coulter, and I. Apodaca, "Improved flux pinning in $YBa_2Cu_3O_7$ with nanorods of the double perovskite $Ba_2YNbO_6$," *Supercond. Sci. Technol.*, vol. 23, Jun. 2010, Art. no. 095004.

[32] G. Ercolano *et al.*, "Strong correlated pinning at high growth rates in $YBa_2Cu_3O_{7-x}$ thin films with $Ba_2YNbO_6$ additions," *J. Appl. Phys.*, vol. 116, 2014, Art. no. 033915.

[33] G. Ercolano *et al.*, "State-of-the-art flux pinning in $YBa_2Cu_3O_{7-\delta}$ by the creation of highly linear, segmented nanorods of $Ba_2(Y/Gd)(Nb/Ta)O_6$ together with nanoparticles of $(Y/Gd)_2O_3$ and $(Y/Gd)Ba_2Cu_4O_8$," *Supercond. Sci. Technol.*, vol. 24, Aug. 2011, Art. no. 095012.

[34] L. Opherden *et al.*, "Large pinning forces and matching effects in $YBa_2Cu_3O_{7-\delta}$ thin films with $Ba_2Y(Nb/Ta)O_6$ nano-precipitates," *Sci. Rep.*, vol. 6, 2016, Art. no. 21188.

[35] M. Sieger *et al.*, "$Ba_2Y(Nb/Ta)O_6$ doped YBCO films on biaxially textured Ni-5at.% W substrates," *IEEE Trans. Appl. Supercond.*, vol. 26, no. 3, Apr. 2016, Art. no. 7500305.

[36] F. Rizzo *et al.*, "Enhanced 77 K vortex-pinning in $YBa_2Cu_3O_{7-x}$ films with $Ba_2YTaO_6$ and mixed $Ba_2YTaO_6$ + $Ba_2YNbO_6$ nano-columnar inclusions with irreversibility field to 11 T," *APL Mater.*, vol. 4, 2016, Art. no. 061101.

[37] P. Pahlke *et al.*, "Thick high $J_c$ YBCO films on ABAD-YSZ templates," *IEEE Trans. Appl. Supercond.*, vol. 25, no. 3, Jun. 2015, Art. no. 6603804.

[38] W. Prusseit, R. Nemetschek, C. Hoffmann, G. Sigl, A. Lümkemann and H. Kinder, "ISD process development for coated conductors," *Phys. C Supercond.*, vol. 426–431, pp. 866–871, 2005.

[39] F. Hengstberger, M. Eisterer, M. Zehetmayer, and H. W. Weber, "Assessing the spatial and field dependence of the critical current density in YBCO bulk superconductors by scanning Hall probes," *Supercond. Sci. Technol.*, vol. 22, Jan. 2009, Art. no. 025011.

[40] B. Maiorov *et al.*, "Synergetic combination of different types of defect to optimize pinning landscape using $BaZrO_3$-doped $YBa_2Cu_3O_7$," *Nature Mater.*, vol. 8, pp. 398–404, 2009.

[41] F. Baca *et al.*, "Control of $BaZrO_3$ nanorod alignment in $YBa_2Cu_3O_{7-x}$ thin films by microstructural modulation," *App. Phys. Lett.*, vol. 94, Mar. 2009, Art. no. 102512.

[42] P. Pahlke *et al.*, "Local orientation variations in YBCO films on technical substrates - a combined SEM and EBSD study," *IEEE Trans. Appl. Supercond.*, vol. 26, no. 3, Apr. 2016, Art. no. 7201505.

[43] M. Sieger *et al.*, "Influence of vicinal substrates on the incorporation of $BaHfO_3$ in thick $YBa_2Cu_3O_{7-\delta}$ films," *IEEE Trans. Appl. Supercond.*, to be published. doi: 10.1109/TASC.2016.2631587.

[44] E. Reich, T. Thersleff, R. Hühne, K. Iida, L. Schultz, and B. Holzapfel, "Structural and pinning properties of $Y_2Ba_4CuMO_y$ (M = Nb, Zr)/$YBa_2Cu_3O_{7-\delta}$ quasi-multilayers fabricated by off-axis pulsed laser deposition," *Supercond. Sci. Technol.*, vol. 22, Aug. 2009, Art. no. 105004.

[45] F. J. Baca, R. L. Emergo, J. Z. Wu, T. J. Haugan, J. N. Reichart, and P. N. Barns, "Microstructural characterization of $YBa_2Cu_3O_{7-x}$ films with $BaZrO_3$ nanorods grown on vicinal $SrTiO_3$ substrates," *IEEE Trans. Appl. Supercond.*, vol. 19, no. 3, pp. 3371–3374, Jun. 2009.

[46] M. Lao *et al.*, "Planar current anisotropy and field dependence of $J_c$ in coated conductors assessed by scanning Hall probe microscopy," *Supercond. Sci. Technol.*, vol. 30, no. 2, Feb. 2017, Art. no. 024004.